A pH-Dependent Aquomet-to-Hemichrome Transition in Crystalline Horse Methemoglobin[†,‡]

Victoria L. Robinson,[§] Benjamin B. Smith,[||] and Arthur Arnone*

Department of Biochemistry, College of Medicine, The University of Iowa, Iowa City, Iowa 52242

Received March 10, 2003; Revised Manuscript Received June 11, 2003

ABSTRACT: In 1947, Perutz and co-workers reported that crystalline horse methemoglobin undergoes a large lattice transition as the pH is decreased from 7.1 to 5.4. We have determined the pH 7.1 and 5.4 crystal structures of horse methemoglobin at 1.6 and 2.1 Å resolution, respectively, and find that this lattice transition involves a 23 Å translation of adjacent hemoglobin tetramers as well as changes in α heme ligation and the tertiary structure of the α subunits. Specifically, when the pH is lowered from 7.1 to 5.4, the Fe^{3+} α heme groups (but not the β heme groups) are converted from the aquomet form, in which the proximal histidine [His87(F8)α] and a water molecule are the axial heme ligands, to the hemichrome (bishistidine) form, in which the proximal histidine and the distal histidine [His58(E7)α] are the axial heme ligands. Hemichrome formation is coupled to a large tertiary structure transition in the eight-residue segment Pro44(CD2)α−Gly51(D7)α that converts from an extended loop structure at pH 7.1 to a π-like helix at pH 5.4. The formation of the π helix forces Phe46(CD4)α out of the α heme pocket and into the interface between adjacent hemoglobin tetramers where it participates in crystal lattice contacts unique to the pH 5.4 structure. In addition, the transition from aquomet α subunits to bishistidine α subunits is accompanied by an ∼1.2 Å movement of the α heme groups to a more solvent-exposed position as well as the creation of a solvent channel from the interior of the α heme pocket to the outside of the tetramer. These changes and the extensive rearrangement of the crystal lattice structure allow the α heme group of one tetramer to make direct contact with an α heme group on an adjacent tetramer. These results suggest possible functional roles for hemichrome formation in vivo.

Initial attempts by Perutz to solve the crystallographic phase problem for proteins involved the swelling and shrinking of hemoglobin crystals (*1*, *2*). One result of this research was the finding that monoclinic crystals of horse methemoglobin can undergo a large pH-dependent transition between two stable lattice forms. At pH 7.1 horse methemoglobin crystallizes in space group *C*2 with unit cell dimensions $a = 108.4$ Å, $b = 63.2$ Å, $c = 54.6$ Å, and $\beta = 110.9°$. When the pH is lowered to 5.4, a considerable increase in unit cell volume occurs because the β angle decreases by 26° (*2*). Since it is now known that a wide range of quaternary structures is energetically accessible to the liganded hemoglobin tetramer (*3*, *4*), the pH 7.1 to 5.4 crystal lattice transition could be due to a large change in quaternary structure. In particular, when crystallized under high-salt conditions at pH 7, horse methemoglobin and liganded human hemoglobin have very nearly the same quaternary structure (the quaternary R structure) (*5*), whereas human carbonmonoxyhemoglobin assumes a significantly different quaternary structure (the quaternary R2 structure) when it is crystallized from poly(ethylene glycol) (PEG)[1] at pH 5.8 (*3*). Therefore, it seemed plausible that the pH 5.4 crystal structure of horse methemoglobin could be another example of a fully liganded mammalian hemoglobin adopting the quaternary R2 structure. However, the results of the X-ray studies described below clearly show that the crystal structure of horse methemoglobin at pH 5.4 remains quaternary R. The increase in unit cell volume is linked instead to coupled changes in α heme ligation and the tertiary structure of the α subunits.

EXPERIMENTAL PROCEDURES

Notation. The notation specifying hemoglobin crystal forms has the following form: protein·ligand·precipitant and pH. The protein codes used in this paper are eHb (equine hemoglobin), hHb (human hemoglobin), tnHb [*Trematomus newnesi* (antarctic fish) hemoglobin], nsHb [nonsymbiotic (rice) plant hemoglobin], scHb (sea cucumber hemoglobin), oMb (ovine myoglobin), and swMb (sperm whale myoglobin). The ligand codes are deoxy, O_2, CO, met (aquomet), bishis (bishistidine), bishis/met (α bishistidine/β aquomet), and CO/bishis (α CO/β bishistidine). The precipitant codes are HS (high salt) and PEG [poly(ethylene glycol)]. The hHb·

[†] This work was supported by Grant GM-58890 from the National Institutes of Health. V.L.R. also was supported by a predoctoral fellowship from The University of Iowa Center for Biocatalysis and Bioprocessing.

[‡] Refined coordinates have been deposited in the Protein Data Bank. The accession numbers for the structures eHb·met·HS7.1 and eHb·bishis/met·HS5.4 are 1NS6 and 1NS9, respectively.

* To whom correspondence should be addressed. E-mail: arthur-arnone@uiowa.edu.

[§] Present address: Center for Advanced Biotechnology and Medicine, Howard Hughes Medical Institute, University of Medicine and Dentistry of New Jersey, 679 Hoes Lane, Piscataway, NJ 08854-5638.

[||] Present address: Department of Radiology, Duke University Medical Center, Durham, NC 27710.

[1] Abbreviations: PEG, poly(ethylene glycol); rms, root mean square; IHP, inositol hexaphosphate.

10.1021/bi030059t CCC: $25.00
Published on Web 08/07/2003

Table 1: Data Collection and Refinement Statistics[a]

	eHb·met·HS7.1	eHb·bishis/met·HS5.4
Data Collection		
space group	*C*2	*C*2
unit cell		
a (Å)	108.4	108.1
b (Å)	63.2	63.4
c (Å)	54.6	53.9
β (deg)	110.9	84.7
asymmetric unit	dimer	dimer
resolution (Å)	1.59	2.07
measurements	186644	125115
unique reflections	42686	21680
completeness (%)	92.3 (75.5)	97.2 (87.7)
$I/\sigma(I)$	13.4 (1.4)	14.3 (4.5)
R_{merge} (%)	4.7 (25.3)	5.3 (12.3)
REFMAC5 Refinement		
R_{cryst} (%)	18.0	16.2
R_{free} (%)	20.0	19.4
water molecules	87	85
rms bond lengths (Å)	0.009	0.012
rms angles (deg)	1.19	1.25
average temp factor (Å^2)	23.2	18.4

[a] The numbers in parentheses for the completeness, $I/\sigma(I)$, and R_{merge} statistics represent values for the outer resolution shell: 2.23−2.07 Å and 1.71−1.59 Å for the eHb·bishis/met·HS5.4 and eHb·met·HS7.1 structures, respectively.

deoxy·HS6.8 (*6*), hHb·O_2·HS6.7 (*7*), and hHb·CO·PEG5.8 (*3*) crystal structures were chosen as the reference T, R, and R2 structures, respectively.

Crystallization and pH Equilibration. Dr. Eric L. Reinerston (Iowa State University Veterinary School, Ames, IA) kindly provided samples of horse blood. Horse hemoglobin was purified and crystallized as specified by Perutz (*8*). Before crystallization, the hemoglobin was deionized using a modified Dintzis column (*9*). Large single crystals grew at room temperature from batch setups containing 2% horse methemoglobin, 1.5 M ammonium sulfate, and 0.35 M ammonium phosphate at pH 7.1. The transition between the neutral and acidic crystal forms was carried out in steps by soaking individual methemoglobin crystals in a series of high ionic strength buffers of progressively lower pH (*2*). Specifically, the pH 7.1 methemoglobin crystals were soaked, for a 24 h time period, in solutions of 3.35 M ammonium sulfate that were buffered with 0.20 M ammonium phosphate at pH 6.6, 6.2, 5.8, and finally 5.4.

Data Collection and Processing. Neutral and low-pH methemoglobin crystals were mounted in quartz capillary tubes, and diffraction data were collected with a Rigaku AFC6R diffractometer that was fitted with a San Diego Multiwire Systems Mark II area detector. A total of 183644 and 125115 reflections were collected for the neutral and acidic crystal forms, respectively. The diffraction data were scaled and merged according to the procedure of Howard et al. (*10*) to give 42686 independent reflections for the eHb·met·HS7.1 data set and 21680 independent reflections for the eHb·bishis/met·HS5.4 data set. Data collection statistics are given in Table 1.

Structure Determination and Refinement. The initial crystal structure of horse aquomethemoglobin at neutral pH, eHb·met·HS7.1, was determined at a resolution of 2.0 Å and refined by real space methods (*11*). This structure recently was used as a starting point to refine a highly isomorphous crystal structure of horse carbonmoxyhemoglobin at pH 8.5, eHb·CO·HS8.5, by restrained least-squares methods to a resolution of 1.9 Å (*4*). Since the eHb·CO·HS8.5 crystal structure was refined by the same procedures used in the present studies, it was used as the starting model to extend the resolution of eHb·met·HS7.1 to 1.6 Å as well as to determine the structure of eHb·bishis/met·HS5.4.

The CO ligands and the highly mobile first three and last four residues of each subunit were removed from the eHb·CO·HS8.5 structure before the molecular replacement methods and rigid-body refinement procedures in the X-PLOR package of programs (*12*) were used to position the asymmetric unit, an $\alpha\beta$ dimer, in the unit cell. This initial atomic model of eHb·met·HS7.1, with temperature factors set to 20 Å^2, had an *R*-value of 23.7% for the data between 8 and 3.5 Å. Stereochemically restrained refinement was carried out initially with the least-squares program PROLSQ (*13*) and then with the program REFMAC5, which uses a maximum likelihood residual and a model for bulk solvent (*14*, *15*). The graphics program TOM/FRODO (*16*, *17*) was used with $F_o - F_c$ electron density omit maps to fit the amino- and carboxy-terminal peptides as well as to make small conformational adjustments to other residues. Bound water molecules were added to the structure by searching the $F_o - F_c$ electron density for peaks greater than 3 times the overall rms density. Putative water molecules that did not have proper stereochemistry were eliminated using the software described by Borgstahl (*18*). The final 1.59 Å structure of eHb·met·HS7.1 includes 87 water molecules and has an *R*-value of 18.0%. After the refinement of the atomic model was completed using all of the diffraction data, a crystallographic R_{free} value of 20.0% was calculated by running 1500 additional cycles of REFMAC5 refinement using only 90% of the diffraction data (*19*). Refinement statistics for this structure, as well as for the eHb·bishis/met·HS5.4 structure, are presented in Table 1.

The eHb·bishis/met·HS5.4 structure was determined and refined in much the same manner as the eHb·met·HS7.1 structure. However, early in the refinement process it was observed that almost no electron density was visible for residues 43 through 50 (the CD corner) of the α subunit, so these 8 residues were omitted from the next round of refinement and then rebuilt in subsequent $F_o - F_c$ electron density maps. In addition, residues 53 through 65 (the E-helix) exhibited a high degree of disorder, and the majority of this section was rebuilt using $F_o - F_c$ omit maps. During the rebuilding process it was discovered that the distal histidine, His58(E7)α,[2] was within bonding distance (2.8 Å) of the heme iron. In most hemoglobin structures, the distal histidine is located about 4 Å from the iron atom. To verify the coordination of the distal histidine to the iron, eight refinement cycles were run on a model that was missing His58(E7)α. A subsequent omit map calculated with the α subunit heme group and the proximal and the distal histidines removed clearly showed the imidazole side chain of the distal histidine positioned 2.2 Å away from the iron atom, replacing a water that normally occupies the sixth coordination site in aquomethemoglobin. After several iterations of PROLSQ

[2] The amino acid residue notation includes the secondary structure position of a residue. Thus His87(F8)α1 locates residue His87α1 as the eight residue of the α1 subunit F-helix.

Table 2: Hemoglobin Quaternary Structure Transitions[a]

transition	Δ_Q (Å)	screw-rotation axis direction angles [α, β, γ (deg)]	screw-rotation axis y-intercept (Å)	screw-rotation angle [ρ (deg)] translation [τ (Å)]
T → eHb·bishis/met·HS5.4	4.5	19.7, 90, 70.3	12.4	−12.2/1.4
T → hHb·O_2·HS6.7 (T → R)	4.7	16.5, 90, 73.5	13.1	−13.5/1.5
T → eHb·met·HS7.1	5.2	13.2, 90, 76.8	17.1	−12.6/1.3
T → hHb·CO·PEG5.8 (T → R2)	9.3	45.3, 90, 44.7	9.2	−24.9/3.1
R → eHb·met·HS7.1	0.8	92.3, 90, 2.3	18.4	−1.0/0.5
R → eHb·bishis/met·HS5.4	1.1	111.5, 90, −21.5	5.1	−2.7/−0.4
R → hHb·CO·PEG5.8 (R → R2)	4.6	81.2, 90, 8.8	5.8	−12.4/1.2
R2 → eHb·met·HS7.1	3.8	84.5, 90, 5.5	3.3	11.2/−0.6
R2 → eHb·bishis/met·HS5.4	3.9	77.3, 90, 12.7	10.1	9.0/−1.7
eHb·met·HS7.1 → eHb·bishis/met·HS5.4	1.0	119.1, 90, −29.1	6.6	−1.5/−0.8

[a] The parameter Δ_Q is a measure of the overall magnitude of a quaternary transition and is defined in the text. The reference T, R, and R2 structures were chosen to be the hHb·deoxy·HS6.8 (*6*), hHb·O_2·HS6.7 (*7*), and hHb·CO·PEG5.8 (*3*) crystal structures, respectively.

refinement and visual refitting of the atomic model, and then REFMAC refinement followed by visual refitting, the final 2.07 Å structure of eHb·bishis/met·HS5.4 included 85 water molecules and had an *R*-value of 16.2%. After the refinement of the atomic model was completed using all of the diffraction data, a crystallographic R_{free} value of 19.4% was calculated by running 1500 additional cycles of REFMAC5 refinement using only 90% of the diffraction data (*19*).

Estimating the Fe−N$^{\epsilon 2}$His and Fe−H_2O Bond Lengths. For both the eHb·met·HS7.1 and eHb·bishis/met·HS5.4 structures a previously described iterative method of refining the Fe−N$^{\epsilon 2}$His and the Fe−H_2O bond lengths was used to eliminate restraint bias (*20*). Normally, these bond distances are refined like all other bond distances with a fixed "ideal" target value as a restraint. In general, these refinement restraints are necessary because the resolution limit for most protein crystals does not permit the free-atom refinement methods used for small molecule crystal structures. However, for diffraction data sets of moderate resolution it should be possible to eliminate the target restraints for a few bond distances in order to obtain an unbiased estimate of their true value. This was accomplished for the Fe−N$^{\epsilon 2}$His and the Fe−H_2O bond lengths by plotting residuals (target value minus refined value) versus target values and then choosing the target value that resulted in a zero residual as the best estimate of the bond distance (see ref *20*).

Structural Analysis. The following criteria were used to identify noncovalent interactions. A polar contact was defined as an atomic interaction of less than 3.2 Å between a pair of polar atoms. A nonpolar contact was defined as an atomic interaction of less than 3.5 Å between two nonpolar atoms or between a polar and a nonpolar atom. Interactions of 3.2−3.5 Å between two polar atoms were counted as nonpolar contacts. A water bridge was defined as a [polar atom···water···polar atom] interaction where both water hydrogen bonds are less than 3.2 Å.

To identify the pH-induced changes in tertiary structure, corresponding subunits of eHb·met·HS7.1 and eHb·bishis/met·HS5.4 were superimposed using an iterative least-squares superposition ("sieve-fit") procedure (*20*) similar to that described by Gerstein and Chothia (*21*). Concerted changes in tertiary structure were identified through the use of δ plots (*20*). Specifically, the magnitude of the main-chain displacement vector, $|\vec{\delta}_n|$, was plotted versus residue number. $|\vec{\delta}_n|$ is defined as

$$|\vec{\delta}_n| = \delta_n = \frac{1}{4n}\left|\sum_{j=1}^{4n} \Delta\vec{r}_j\right|$$

where $\Delta\vec{r}_j$ is the atomic displacement vector for the *j*th main-chain atom of the *n*-residue peptide, and the summation is carried out over *n* contiguous residues. A peptide size of 1 was chosen in this study because the direction of $\Delta\vec{r}$ changes rapidly from residue to residue in the region of the α CD corner.

Rigid-body screw rotation analysis (*5*, *22*) was used to characterize quaternary structure transitions between pairs of hemoglobin tetramers. The details of this approach have been described by Mueser et al. (*4*). In brief, the following steps are involved. First, each tetramer was placed in a standard orientation with the dyad axis of the tetramer positioned along the *y*-axis of the coordinate system. Next, the backbone atomic coordinates of the $\alpha 1\beta 1$ and $\alpha 2\beta 2$ dimers[3] of each tetramer were averaged about the dyad axis. Then the sieve-fit least-squares procedure was used to superimpose the $\alpha 1\beta 1$ dimers of a pair of hemoglobin tetramers and to identify the backbone atoms of the $\alpha 1\beta 1$ "static core" (*4*, *21*). As a global measure of the magnitude of a quaternary structure difference, the parameter Δ_Q (Table 2) was defined as the rms deviation of the nonsuperimposed $\alpha 2\beta 2$ static core backbone atoms. Finally, the $\alpha 2\beta 2$ dimers were superimposed, and the set of screw rotation parameters associated with this second superposition was used to define the change in quaternary structure (Table 2). Only four independent parameters are required to uniquely specify the screw rotation transformation (*4*): one direction angle of the screw rotation axis (α or γ), the *y*-intercept of the screw rotation axis, the angle of rotation ρ, and the translation distance τ.

RESULTS

Changes in the Crystal Lattice Structure. Soaking protein crystals in buffers of different pH normally does not result in very large structural changes (e.g., see refs *23* and *24*). In the case of horse methemoglobin, however, reducing the pH of crystals grown at neutral pH to below 6.0 results in a

[3] The notation $\alpha 1\alpha 2$, $\beta 1\beta 2$, $\alpha 1\beta 1$, $\alpha 2\beta 2$, $\alpha 1\beta 2$, and $\alpha 2\beta 1$ refers to the six subunit−subunit pairings within the $\alpha_2\beta_2$ hemoglobin tetramer.

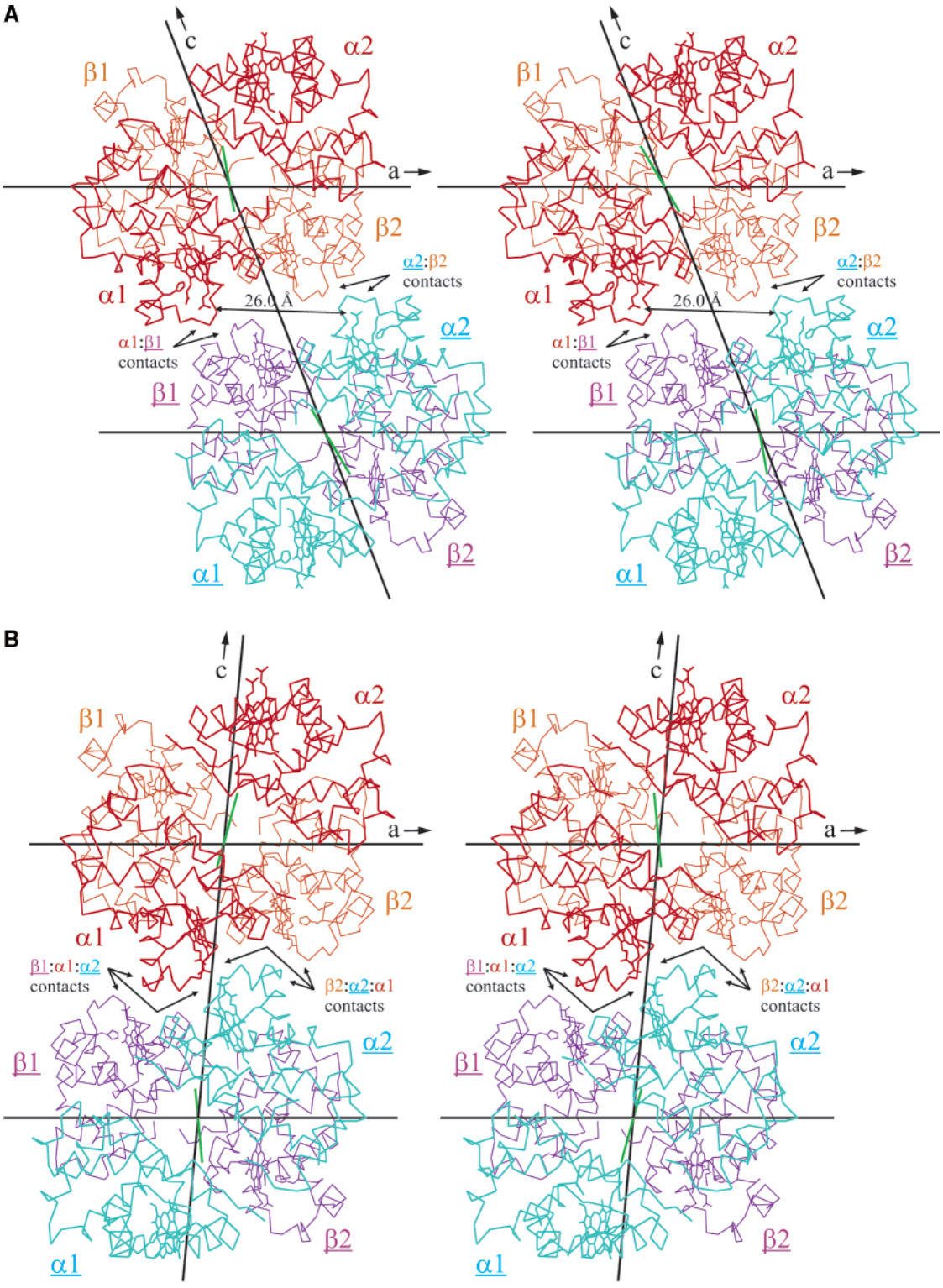

FIGURE 1: Stereo diagrams showing the crystal lattice contacts of two adjacent hemoglobin tetramers in the eHb·met·HS7.1 crystal structure (A) and the eHb·bishis/met·HS5.4 crystal structure (B). The unit cell *a*- and *c*-axes are labeled, and the *b*-axis is color-coded in green. In both structures an $\alpha 1\beta 1$ dimer is the asymmetric unit, and the molecular dyad of each $\alpha_2\beta_2$ tetramer is coincident with a crystallographic 2-fold symmetry axis that runs along the *b*-axis of the unit cell. A second, parallel crystallographic 2-fold axis (not labeled or color-coded) is midway between the two tetramers, and in the eHb·bishis/met·HS5.4 structure it passes through a propionic acid-propionic acid hydrogen bond. The upper tetramer (red, α subunits, and orange, *β* subunits) is related to the lower tetramer (cyan, α subunits, and purple, *β* subunits with underlined subunit labels) by a translation of one unit cell repeat along the *c*-axis. The angle between the *a*- and *c*-axes is 110.9° in the eHb·met·HS7.1 crystal lattice and 84.7° in the eHb·bishis/met·HS5.4 crystal lattice, a change that results in a very large (~23 Å) relative movement of the two adjacent tetramers. This figure and the other stereo atomic model diagrams were prepared with the program DISPLA (*65*).

large increase in unit cell volume (*1*, *2*) and, we now find, very interesting structural changes. The key lattice contacts associated with this pH-dependent transition occur between two $\alpha_2\beta_2$ tetramers that are related by a translation of one repeat distance along the *c*-axis of the unit cell (Figure 1). The subunits of the second (the translated) tetramer are

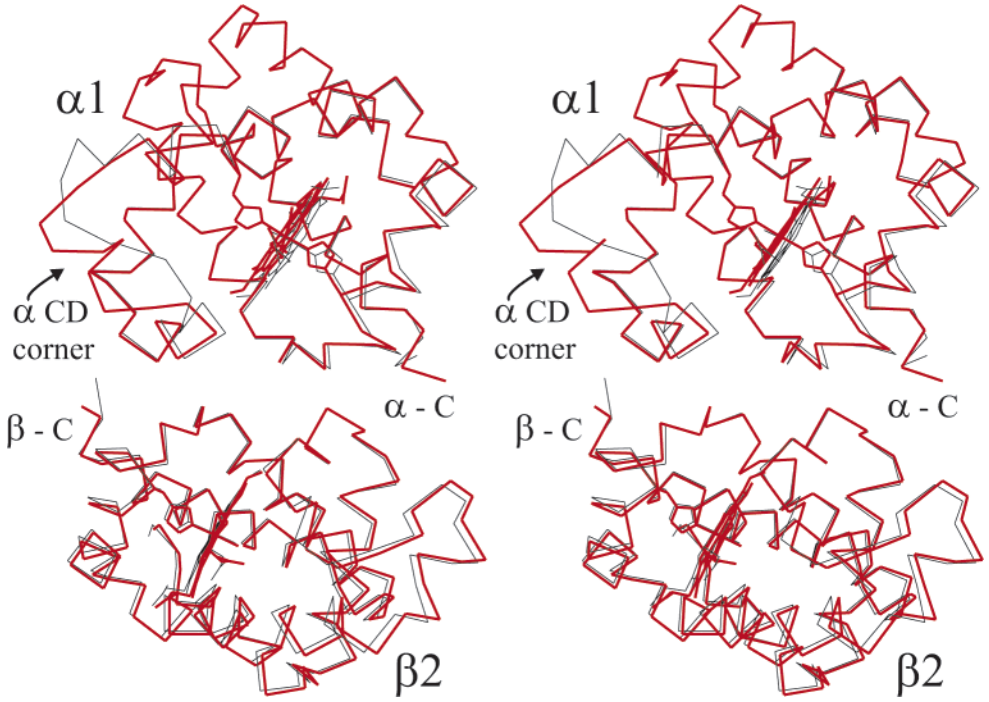

FIGURE 2: Stereo plots of α-carbon tracings of the α1 and *β*2 subunits of eHb·met·HS7.1 (black lines) and eHb·bishis/met·HS5.4 (red lines). The backbone atoms of the α1*β*1 dimers of the two structures were superimposed using the sieve-fit algorithm described in the text. The high level of overlap between the *β*2 subunits of eHb·met·HS7.1 and eHb·bishis/met·HS5.4 shows that the two structures have nearly identical quaternary structures. Note the formation of a hemichrome complex as well as the transition of the CD corner from an extended loop to a helix in the α subunit of the eHb·bishis/met·HS5.4 structure.

identified by underlined subunit labels in the analysis that follows.

The crystals used in this study have space group symmetry *C*2 with one dimer as the asymmetric unit (*1*). The molecular dyad of each hemoglobin $\alpha_2\beta_2$ tetramer coincides with a crystallographic 2-fold axis that runs along the *b*-axis of the unit cell (Figure 1). In the eHb·met·HS7.1 crystal structure (Figure 1A), one small set of three nonpolar intertetramer lattice contacts forms between α1 residues Pro44(CD2)α1 and His45(CD3)α1 and *β*1 residues Ser44(CD3)*β*1, Pro58(E2)*β*1, and Lys59(E3)*β*1. In contrast, and as discussed more fully below, a very different and much more extensive set of polar and nonpolar lattice interactions forms between tetramers in the eHb·bishis/met·HS5.4 crystal structure (Figure 1B).

The pH-induced change in lattice contacts results in a very large movement of hemoglobin tetramers within the crystal lattice. At pH 7.1, the angle between the unit cell *a*- and *c*-axes is 110.9°, and the heme propionates on the α1 and α2 subunits of adjacent tetramers are no closer than 26.0 Å (Figure 1A). At pH 5.4, the angle between the *a*- and *c*-axes is reduced to 84.7° and the α heme propionic acid groups on adjacent tetramers move more than 23 Å toward each other to form an intertetramer hydrogen bond (Figure 1B). This clearly demonstrates a very high degree of crystal lattice fluidity, and it indicates that one or both of the interacting propionic acid carboxyl groups are protonated at pH 5.4.

Lack of Quaternary Structure Change. Because a wide range of quaternary structures is energetically accessible to the fully liganded hemoglobin tetramer (*3*, *4*), it was very possible that the pH-induced transition in crystalline horse methemoglobin could be due to a large change in quaternary structure. In fact, in an earlier publication it was hypothesized that this transition was the result of a shift from the quaternary R to the quaternary R2 structure (*3*). This, however, is not the case. The data in Table 2 show that both the neutral pH and the pH 5.4 methemoglobin structures have essentially the same R-like quaternary structure. The parameters for the R → eHb·met·HS7.1, R → eHb·bishis/met·HS5.4, and eHb·met·HS7.1 → eHb·bishis/met·HS5.4 rigid-body transitions (i.e., the Δ_Q values and screw rotation parameters) show there are only small differences between the quaternary structures of eHb·met·HS7.1, eHb·bishis/met·HS5.4, and the reference R structure (hHb·O_2·HS6.7). Similarly, analysis relative to the quaternary T structure of deoxyhemoglobin shows that the T → eHb·met·HS7.1 and T → eHb·bishis/met·HS5.4 rigid-body transitions are almost identical to the reference T → R transition, not the reference T → R2 transition.

Figure 2 compares the quaternary structures of the eHb·Met·HS7.1 and eHb·bishis/met·HS5.4 structures by displaying the degree of overlap in the positions of their *β*2 subunits after the corresponding α1*β*1 dimers have been superimposed. The negligible deviation in the positions of the nonsuperimposed *β*2 subunits of the eHb·bishis/met·HS5.4 and eHb·met·HS7.1 atomic models again illustrates the high level of quaternary isomorphism between these structures.

Hemichrome Formation. At the heart of the crystal lattice changes is an unexpected exchange of α heme ligands that is very obvious in our electron density maps (Figure 3). At pH 7.1, the α and *β* subunits of horse methemoglobin exist in the normal aquomet form with the proximal histidine [His87(F8)α or His92(F8)*β*] and a water molecule serving as the axial heme ligands. However, when the pH is reduced to 5.4, the Fe^{3+} α heme groups (but not the *β* heme groups) are converted from the aquomet form to the hemichrome (bishistidine) form in which the proximal histidine and the

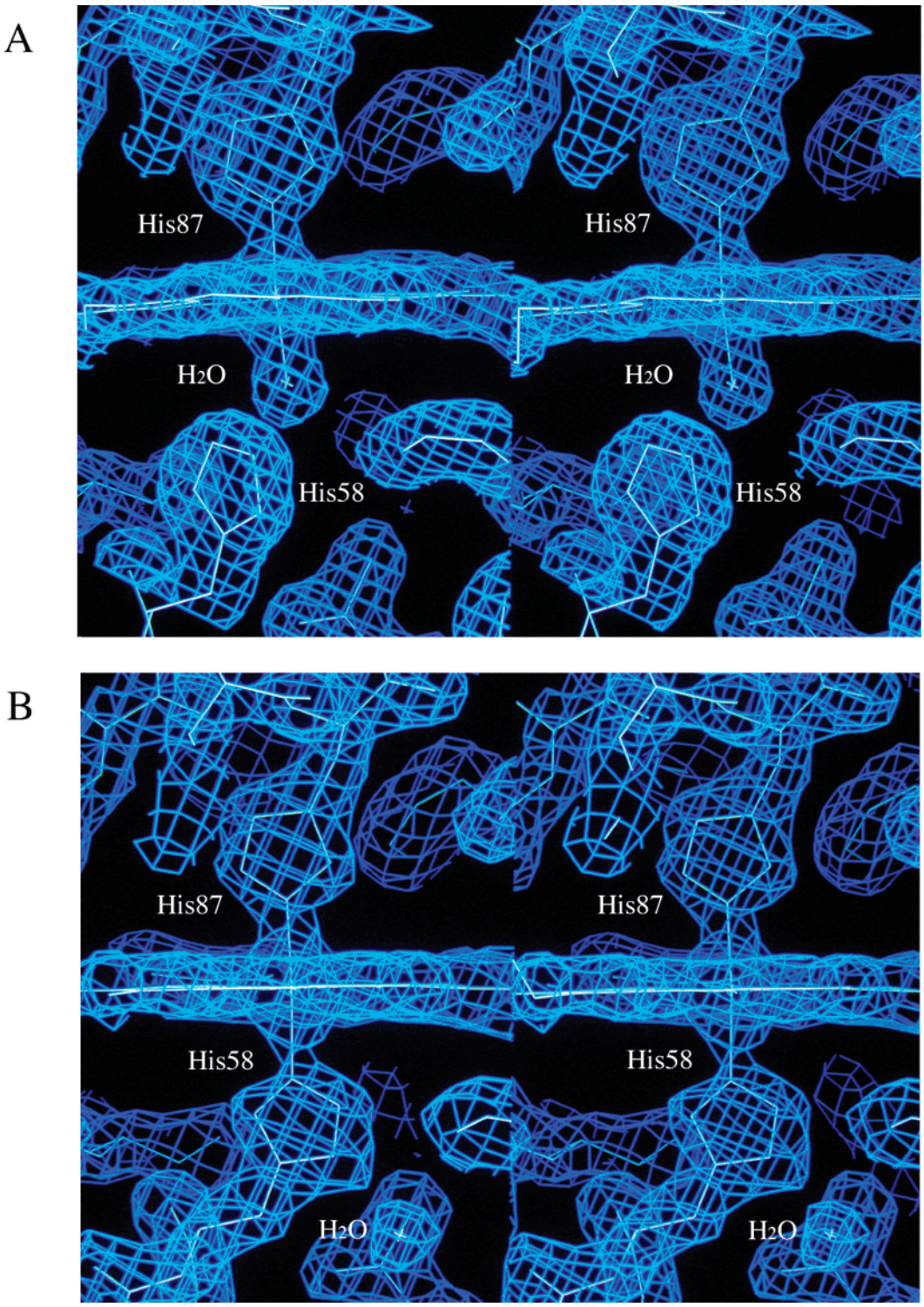

FIGURE 3: Stereo plots of $2F_o - F_c$ electron density in the region of the aquomet α heme group of eHb·met·HS7.1 (A) and the hemichrome α heme group of eHb·bishis/met·HS5.4 (B). The electron density contours are drawn at 1.4 times the rms density of the entire map. The water molecule in (B) is unique to the eHb·bishis/met·HS5.4 structure and forms part of a water channel that is shown more fully in Figure 4B. The β heme groups for both the eHb·met·HS7.1 and eHb·bishis/met·HS5.4 structures are in the aquomet state with electron density (not shown) very similar to that of the α heme group of eHb·met·HS7.1 in (A). The figures were prepared with the graphics program TOM/FRODO (*16*, *17*).

distal histidine [His58(E7)α] are the axial heme ligands (Figure 3).

Three crystal structures of naturally occurring hemichrome hemoglobins have been reported to date: a 2.5 Å structure of a monomeric hemichrome hemoglobin from the sea cucumber *Caudina arenicola* (scHb·bishis·PEG8.0) (*25*), a 2.4 Å structure of a homodimeric hemichrome hemoglobin from rice (nsHb·bishis·HS7.8) (*26*), and a 2.0 Å structure of an $\alpha_2\beta_2$ tetrameric hemoglobin from the antarctic fish *T. newesi* in which the α subunits have a CO ligand and the β subunits are in the hemichrome form (tnHb·CO/bishis·PEG7.4) (*27*). In addition, site-directed mutagenesis has been used to produce a variant form of pig myoglobin [oMb-(H64V/V68H)·bishis·HS7.1] that was found to have bish-

Table 3: Heme Stereochemistry[a]

structure	Fe-to-heme plane distance (Å)	proximal Fe−HisN$^{\epsilon 2}$ bond length (Å)	distal Fe−ligand bond length (Å)	proximal histidine tilt angle (deg)	distal histidine tilt angle (deg)	resolution (Å)	ref
hHb·deoxy·HS6.8	−0.62, −0.43	2.17, 2.22		86.8, 87.9		1.5	*6*
hHb·CO·PEG5.8	−0.04, −0.07	2.11, 2.10	1.77, 1.76	82.8, 86.0		1.7	*3*
eHb·met·HS7.1	−0.13, −0.11	2.14, 2.19	2.15, 2.15	88.5, 86.5		1.6	this paper
eHb·bishis/met·HS5.4	0.04, −0.08	2.11, 2.16	2.18, 2.04	83.1, 87.1	67.6 (α)	2.1	this paper
tnHb·CO/bishis·PEG7.4	−0.12, 0.08	2.06, 2.00	1.86, 2.00	89.0, 82.2	73.0 (*β*)	2.0	*27*
nsHb·bishis·HS7.8	0.07	2.09	2.06	88.1	87.1	2.4	*26*
scHb·bishis·PEG8.0	0.07	2.06	2.07	89.3	77.0	2.5	*25*
oMb(H64V/V68H)·bishis·HS7.1	−0.07	2.20	2.29	82.7	57.1	2.1	*28*
swMb·met·HS7.0	−0.14	2.14	2.13	87.0		1.1	*30*
swMb·O_2·HS7.0	−0.09	2.06	1.81	89.0		1.0	*30*

[a] In the case of the entries for the first five tetrameric hemoglobin structures, the first and second numbers are values for the α and *β* subunits, respectively. The Fe-to-heme plane distance is negative when the Fe atom is on the proximal side of the heme plane. The proximal or distal histidine tilt angle is the acute angle between the plane of the imidazole ring and the heme plane. Distal histidine tilt angles are listed only for the bishistidine structures. The heme plane is defined (in this table) as the least-squares plane of the 24-atom porphyrin macrocycle. For the eHb·met·HS7.1 and eHb·bishis/met·HS5.4 structures, the Fe−HisN$^{\epsilon 2}$ and Fe−ligand bond lengths were obtained by adjusting the REFMAC5 target values until they matched the corresponding refined bond lengths [see Kavanaugh et al. (*20*)].

istidine heme ligation (*28*). In this case, however, the double mutation in which the distal histidine, His64(E7), is replaced with valine and Val68(E11) is replaced with histidine resulted in an unusual His68(E11)−heme linkage.

Listed in Table 3 are some fundamental parameters of heme stereochemistry for the published bishistidine−globin structures, the eHb·met·HS7.1 and eHb·bishis/met·HS5.4 structures, and some other high-resolution hemoglobin and myoglobin structures. The most accurate of these parameters is the displacement of the Fe atom from the heme plane because the heme plane is defined as the least-squares plane of the large 24-atom porphyrin macrocycle, and the electron-dense Fe atom can be precisely positioned. In the case of the five-coordinate hemes of deoxyhemoglobin, the Fe atom is out of the heme plane on the proximal side by 0.62 and 0.43 Å for the α and *β* subunits, respectively. The Fe atom also is out of the heme plane on the proximal side, albeit to a much lesser extent, for all of the non-hemichrome liganded forms of hemoglobin and myoglobin. This reflects the dominant influence of the tethered proximal histidine ligand over the smaller untethered distal ligands. In the hemichrome α subunits of eHb·bishis/met·HS5.4, however, the Fe atom is pulled through the heme plane by a small amount to the distal side, indicating the distal histidine−Fe interaction is at least as strong as the proximal histidine−Fe interaction. This is also the case for the *β* subunits of tnHb·CO/bishis·PEG7.4, both subunits of nsHb·bishis·HS7.8, and the single subunit of scHb·bishis·PEG8.0. The only exception is the oMb(H64V/V68H)·bishis·HS7.1 structure where the Fe atom remains on the proximal side of the heme plane. This is consistent with the NMR results of Qin et al. (*29*) indicating that "the axial bond to the distal His68(E11) is weakened or strained as compared with that for the proximal His93(F8)".

Because the structure of swMb·met·HS7.0 (*30*) was determined at near-atomic (1.1 Å) resolution and refined without heme restraints, it is likely to depict the heme stereochemistry of a "normal" aquomet subunit very accurately. With this assumption, the refined values of most of the heme parameters for the eHb·met·HS7.1 and eHb·bishis/met·HS5.4 aquomet subunits can be classified as normal (see Table 3). For example, the proximal histidine−Fe bond lengths in the α and *β* aquomet subunits of eHb·met·HS7.1 and the *β* aquomet subunit of eHb·bishis/met·HS5.4 are probably within experiment error of the 2.14 Å value in the swMb·met·HS7.0 structure. The α proximal and α distal histidine−Fe bond lengths in eHb·bishis/met·HS5.4 are also close to 2.14 Å, again indicating that these histidine−Fe bonds are of comparable strength. In addition, the distal Fe−H_2O bond lengths in the eHb·met·HS7.1 α and *β* subunits are very nearly equal to the 2.13 Å value of the Fe−H_2O bond length in the swMb·met·HS7.0 structure. The only exception is the *β* subunit Fe−H_2O bond in eHb·bishis/met·HS5.4. Since it is significantly shorter (2.04 Å) than the corresponding swMb·met·HS7.0 and eHb·met·HS7.1 bonds, it appears to be strengthened at low pH.

The proximal and distal Fe−ligand bond lengths of the eHb·bishis/met·HS5.4 structure show small differences relative to the corresponding bond lengths in the other bishistidine structures (Table 3). These may be real differences in heme stereochemistry, or they may simply reflect differences in the resolution of the diffraction data or in refinement methods. However, the severe tilt angle of the distal histidine (i.e., its large deviation from the optimal value of 90°) in the oMb(H64V/V68H)·bishis·HS7.1 structure is clearly a real difference that is consistent with the weakened, long distal histidine−Fe bond (*29*) and the fact that the Fe atom is on the proximal side of the heme plane. In fact, there is a rough correlation in four of the bishistidine structures [oMb(H64V/V68H)·bishis·HS7.1, eHb·bishis/met·HS5.4, scHb·bishis·PEG8.0, and nsHb·bishis·HS7.8] between the tilt angle of the distal histidine, the degree to which the Fe atom is shifted to the distal side of the heme plane, and the length of the distal histidine−Fe bond. A tilt angle closer to 90° results in a stronger distal histidine−Fe bond (with a shorter bond length) that pulls the Fe atom increasingly out of the heme plane on the distal side.

Changes in Secondary and Tertiary Structure. Despite the high degree of quaternary structure similarity between eHb·met·HS7.1 and eHb·bishis/met·HS5.4, at low pH a major change in secondary structure is induced in the α subunit CD corner of equine methemoglobin (Figures 2 and 4). In the eHb·met·HS7.1 structure, as in all of the other tetrameric hemoglobin structures reported to date, the residues of the α CD corner form an extended loop with ϕ/ψ angles mostly at the top of the upper-left quadrant of Ramachandran space (Figure 5). This loop includes two *β*-turns (*31*): a type I

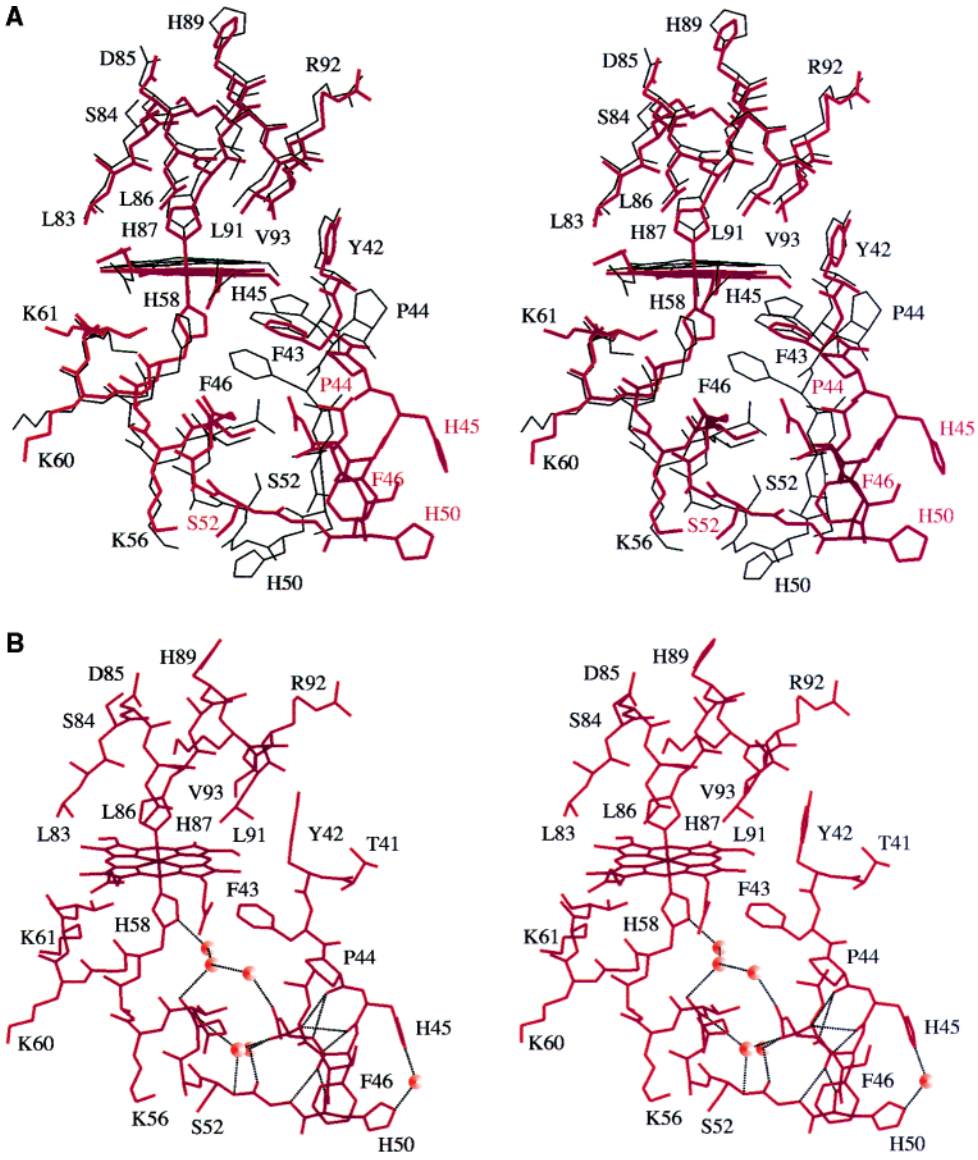

FIGURE 4: (A) Stereo plots of the α heme regions of eHb·met·HS7.1 (black lines) and eHb·bishis/met·HS5.4 (red lines). The α subunit main-chain atoms of the two structures were superimposed using the sieve-fit algorithm described in the text. (B) Stereo plot of the α heme region of eHb·bishis/met·HS5.4. Water molecules forming intrasubunit interactions are shown as filled circles. Hydrogen bonds are drawn with black dotted lines.

β-turn centered at residues Pro44(CD2)α and His45(CD3)α and a type II β-turn centered at residues His50(D1)α and Gly51(D7)α (Figure 4A). Remarkably, in the eHb·bishis/met·HS5.4 structure the CD corner is transformed to a helix (Figures 2 and 4). The ϕ/ψ angles of residues 45−50 shift to the helical region of Ramachandran space with residues His45(CD3)α, Phe46(CD4)α, and Asp47(CD6)α having the ϕ/ψ angles of an α-helix and residues Leu48(CD7)α, Ser49-(CD8)α, and His50(D1)α having the ϕ/ψ angles of a more extended helix (Figure 5). The pattern of ϕ/ψ angles and the fact that residues Phe46(CD4)α and Gly51(D7)α are connected by a ($i \leftarrow i + 5$) hydrogen bond (Figure 4B) indicate that residues 46−51 fit the definition of a $\pi_{\alpha R}$-turn (*32*) and residues 45−49 fit the definition of the first five residues of a π-helix (*33*).

The magnitudes of the pH-induced conformational changes were determined by calculating the atomic displacements, the δ values, between main-chain atoms after the corresponding subunits of eHb·met·HS7.1 and eHb·bishis/met·HS5.4 were superimposed. The δ plot of the α subunits is dominated by two large peaks that exceed 6 Å in magnitude (Figure 6A). One peak is centered at residue His45(CD3)α and the other at His50(D1)α, reflecting the β-turn to helix transition described above. In eHb·met·HS7.1 these histidine residues are located at either end of the CD corner loop and come no closer than 13.1 Å. However, in eHb·bishis/met·HS5.4, His45(CD3)α and His50(D1)α are on the same side of the short "CD helix". The $N^{\epsilon 2}$ atoms of these two histidines now are separated by only 4.2 Å, and both are hydrogen-bonded to a tightly bound water molecule that forms a bridge between them (Figure 4B).

Helix formation at the CD corner creates voids and disrupts the close-packed environment on the distal side of the α-heme group. Particularly disruptive is the displacement of Phe46(CD4)α, which is expelled from the hydrophobic interior of the heme pocket and forced into the environment of the pH 5.4 crystal lattice interface. The voids created by the helix formation and the displacement of Phe46(CD4)α

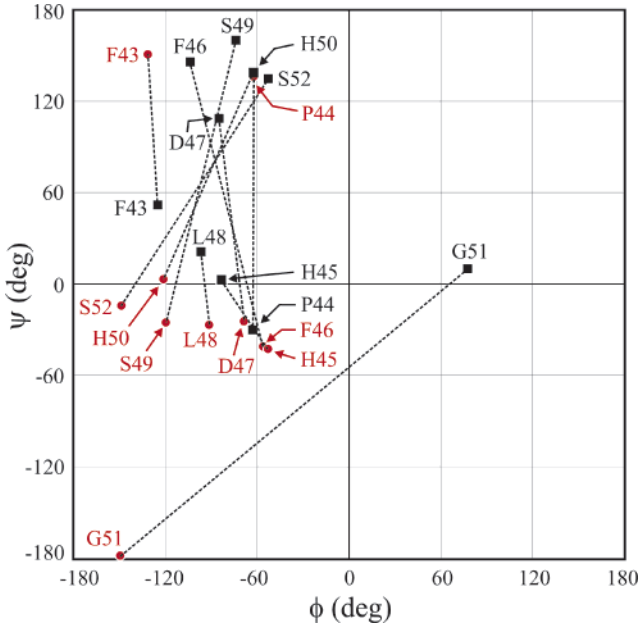

FIGURE 5: Ramachandran plot displaying the ϕ/ψ angles of the α subunit CD corner of eHb·met·HS7.1 (black squares and labels) and eHb·bishis/met·HS5.4 (red circles and labels). Dashed lines connect the (ϕ/ψ) coordinates of corresponding residues in the two structures.

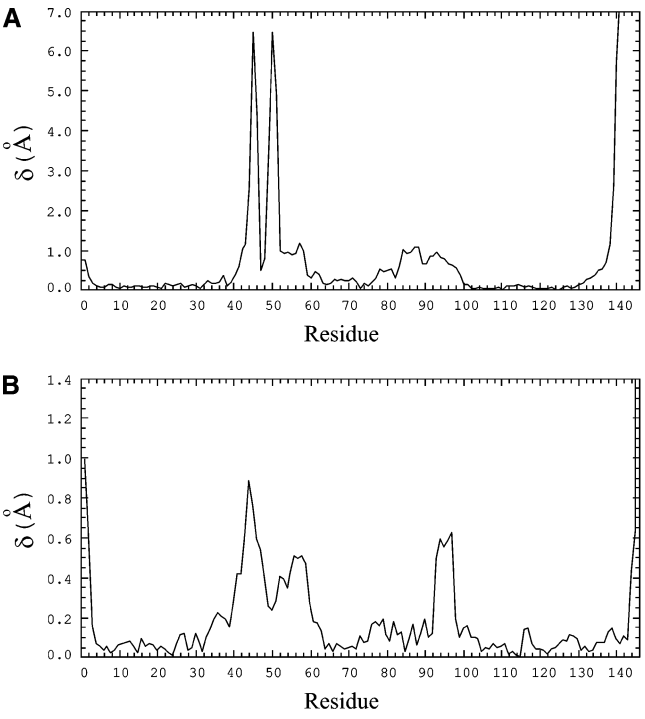

FIGURE 6: δ plot of the main-chain displacements of the α subunits (A) and the β subunits (B). Subunit backbone atoms of eHb·met·HS7.1 and eHb·bishis/met·HS5.4 were superimposed using the sieve-fit algorithm described in the text.

are filled by water molecules (Figure 4B). In particular, three well-resolved water molecules link together to create a hydrogen-bonded solvent channel extending from the distal histidine to the exterior of the protein. Two other water molecules fill the void of the displaced side chain of Ser52(E1)α and form intrasubunit water bridges that link the CD corner with the NH_2 terminus of the E-helix.

The superimposed α subunits in Figure 4A and the δ plot in Figure 6A also show that the first seven residues of the α E-helix (residues 52−58) are shifted toward the heme by about 1 Å. These structural differences are not due to a rearrangement of backbone atoms but result from a rigid-body movement of the first third of the E-helix in response to hemichrome formation and the transition that occurs in the CD corner. The additional small δ peak centered at Gly57(E6)α is due directly to the formation of the hemichrome. Hemichrome formation also leads to a very significant displacement of the heme itself and to associated structural perturbations on the proximal side of the α heme. As shown in Figure 7, relative to the position of the α heme in eHb·met·HS7.1, the α heme in eHb·bishis/met·HS5.4 is displaced by about 1.2 Å to a more solvent-exposed position. This in turn results in shifts of 0.5−1.2 Å in the tethered α F-helix (residues 80−88), the α FG corner (residues 89−93), and the beginning of the α G-helix (residues 94−98) (Figures 4A, 6A, and 7).

There is a direct structural link between the FG corner and the COOH-terminal residues of the α subunit (*20*, *34*, *35*). In the eHb·met·HS7.1 crystal structure the phenolic group of Tyr140(HC2)α is packed tightly into a pocket composed of residues from the α1 F-helix, α1 FG corner, and the β2 subunit C-helix. This formation is stabilized by hydrogen bonding of the Tyr140(HC2)α hydroxyl group with the backbone carbonyl oxygen and nitrogen of Val93(FG5)α. In the eHb·bishis/met·HS5.4 structure the COOH-terminal tripeptide rotates in conjunction with the F-helix movement. Although the interaction between the hydroxyl group of Tyr140(HC2)α and backbone carbonyl oxygen of Val93(FG5)α is maintained, Tyr140(HC2)α assumes a different orientation, and the backbone atoms of the mobile COOH-terminal dipeptide shift by more than 7 Å (Figure 6A).

In contrast to the extensive tertiary structural transformations observed in the α subunit of the eHb·bishis/met·HS5.4 structure, only modest conformational changes in β subunit tertiary structure are observed, with most of the features in the β subunit δ plot (Figure 6B) having magnitudes of less than 1.0 Å. They reveal backbone movements of the β NH_2-terminal tripeptide, residues 41−48β, residues 52−59β, residues 93−97β, and the β COOH-terminal tripeptide. The NH_2- and COOH-terminal movements are due most likely to changes in the state of protonation of the NH_2-terminal amino group and the side chain of the COOH-terminal residue, His146(HC3)β. In particular, the main-chain atoms of each β COOH terminus move 4.5 Å toward each other across the central solvent channel. His146(HC3)β1 and His146(HC3)β2 are 25 Å apart in the eHb·met·HS7.1 structure but only 13 Å apart in the eHb·bishis/met·HS5.4 structure where they are positioned inside the solvent channel that runs through the center of the hemoglobin tetramer. The 0.9 Å δ plot peak centered at Ser44(CD3)β is a consequence of a lattice contact involving Asp43(CD2)β and adjacent residues (see below). The small structural change (less than 0.5 Å) in the 52−59β peptide is a rigid-body movement of the main-chain atoms of the exterior β D-helix and the beginning of the β E-helix, not a gross reorganization of tertiary structure. This is probably a secondary perturbation originating from the Asp43(CD2)β lattice contact. That is, the perturbations of the CD corner propagate through the main-chain atoms of the D-helix and into the first few residues of the E-helix. Finally, the 0.4−0.6 Å shift of β FG corner residues 93−97β is due primarily to their

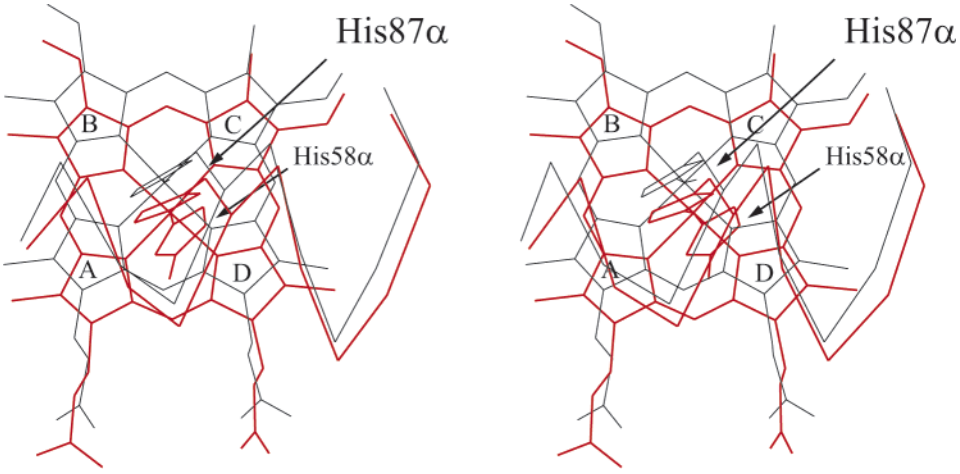

FIGURE 7: Stereo plot of the α heme regions of eHb·met·HS7.1 (black lines) and eHb·bishis/met·HS5.4 (red lines) superimposed as in Figure 4A. The heme groups have been rotated approximate 90° relative to their positions in Figure 4A.

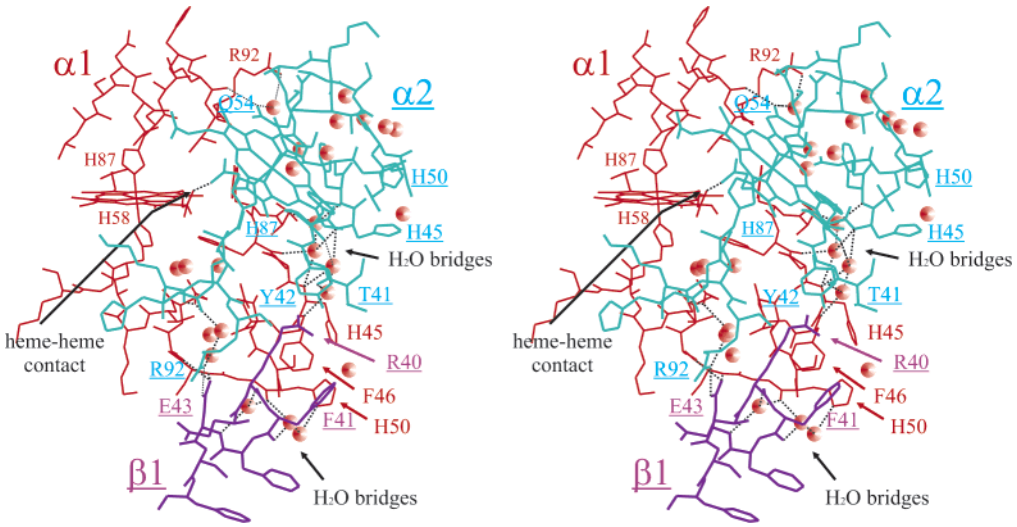

FIGURE 8: Enlarged stereoview of the eHb·bishis/met·HS5.4 lattice contact shown in Figure 1B. Water molecules are shown as filled circles. Intertetramer hydrogen bonds are drawn with black dotted lines. Labeling and color coding are as in Figure 1B, and spatial orientation is as in Figure 4.

interaction with the altered β COOH-terminal dipeptide as well as to their contact with α C-helix residues (which undergo structural change as described above) across the α1β2 interface.

Lattice Contacts. Some key intertetramer interactions that stabilize the eHb·bishis/met·HS5.4 crystal lattice are shown in Figure 8. In particular, the protruding phenyl ring of Phe46(CD4)α participates in a stack of π−cation interactions between adjacent tetramers, with the positively charged guanidinium ion of Arg40(C6)β1 sandwiched between (and less than 3.6 Å from) the electron-rich aromatic rings of Phe46(CD2)α1 and Tyr42(C7)α2. These π−cation interactions could each contribute more than 3 kcal/mol to the stabilization of the eHb·bishis/met·HS5.4 crystal lattice (*36*). In addition to the π−cation interactions, a series of intertetramer water bridges create a "latticework" of hydrogen bonds between one tetramer and its neighbor. A string of four water molecules connect polar backbone atoms of residues Thr41(C6)α1, Phe43(CD1)α1, His45(CD3)α1, and Phe46(CD4)α1 with those of symmetry-related residues Phe46(CD4)α2, His45(CD3)α2, Phe43(CD1)α2, and Thr41(C6)α2 in an antiparallel fashion. Three other water molecules connect the side chain and the carbonyl oxygen of His50(D1)α1 with polar backbone atoms of residues Arg40(C6)β1, Phe41(C7)β1, and Asp43(CD2)β1. Finally, a complicated network of hydrogen bonds involving the side chains of Gln54(E3)α1, Arg92(FG4)α2, and Asp43(CD2)β1, some polar backbone atoms, and a water molecule connects subunits α1, β1, and α2 (see Figure 8).

Heme-Accessible Surface Area. The pH-induced conformational changes result in a large increase in the accessible surface area of the heme group (Figures 4A and 7). In the eHb·met·HS7.1 structure, the heme groups of the α subunits have 121 Å^2 of surface exposed to solvent. In isolated tetramers of eHb·bishis/met·HS5.4, however, 198 Å^2 of each α subunit heme (fully one-fourth of the ~800 Å^2 total surface area of a heme group) is interacting with solvent. This is due to the void that is created by the loss of several heme−protein interactions and to the large shift of the heme itself (Figures 4A and 7). Helix formation at the α CD corner of the eHb·bishis/met·HS5.4 structure completely removes Phe46(CD4)α from the heme pocket and causes Phe43(CD1) to slide partly out of the heme pocket. In addition, the large movement of His45(CD3)α removes it from ionic contact with the propionic acid group of pyrrole D. These changes cause the C and D pyrrole rings of the heme group to drop

slightly toward the void that has been created on the distal side of the heme pocket (Figure 4A). The large 1.2 Å outward movement of the α heme group is linked more directly to hemichrome formation and its tethering to His58(E7)α. Together, these changes lead to increases of 58 and 14 Å^2 in the accessible surface area of pyrrole rings D and A, respectively, which accounts for almost all of the 77 Å^2 increase in heme surface area.

DISCUSSION

Comparison with Other Hemichrome Structures. As noted above, crystal structures of naturally occurring hemichrome hemoglobins have been reported for the monomeric invertebrate hemoglobin from the sea cucumber *C. arenicola* (scHb·bishis·PEG8.0) (*25*), the homodimeric plant hemoglobin from rice (nsHb·bishis·HS7.8) (*26*), and the tetrameric vertebrate hemoglobin from the antarctic fish *T. newesi* in which the α subunits have a CO ligand and the *β* subunits are in the hemichrome form (tnHb·CO/bishis·PEG7.4) (*27*). The eHb·bishis/met·HS5.4 structure of liganded equine hemoglobin reported in this paper is the first crystal structure of a hemichrome complex in a mammalian hemoglobin molecule.

Although all of these hemoglobin molecules display the same basic globin fold, they have significantly different primary structures (with amino acid identities of less than 20% between most pairs of sequences), they were crystallized under very different solution conditions, and their crystal lattices are characterized by very different intermolecular contacts. Despite these differences, the plant, invertebrate, vertebrate, and mammalian hemichrome crystal structures all exhibit two similar hemichrome-induced structural characteristics: a shift of the heme group to a more exposed position and a narrowing of the heme pocket. As discussed above, the α heme group of eHb·bishis/met·HS5.4 is positioned approximately 1.2 Å further out of the heme pocket than it is in eHb·met·HS7.1, a movement that increases its solvent-accessible surface area by ∼80 Å^2. Similarly, Mitchell et al. (*25*) found that the heme group of scHb·bishis·PEG8.0 is "approximately 2.0 Å further out of the heme pocket", and an ∼1 Å movement of the hemichrome heme group toward the solvent was also described in the other two published structures of naturally occurring hemichrome hemoglobins, nsHb·bishis·HS7.8 (*26*) and tnHb·CO/bishis·PEG7.4 (*27*). Likewise, in all four of these structures the heme pocket narrows as the E- and F-helices move closer together.

The shift in heme position and the narrowing of the heme pocket are clearly required for the formation of the distal hemichrome bond with residue E7. In aquomet subunits the distal histidine N$^{\epsilon 2}$ atom is located approximately 4.3 Å away from the heme iron. Therefore, to coordinate with the iron, the distal histidine and the heme center must move toward each other by ∼2 Å. This is accomplished by the shift of the heme group and the narrowing of the heme pocket as the E- and F-helices move toward each other. It is interesting to note that these movements do not occur in the mutant myoglobin oMb(H64V/V68H)·bishis·HS7.1, where the hemichrome coordination is with residue E11 instead of E7 (*28*). Residue E11 is located ∼2 Å closer to the heme Fe atom than is residue E7 because it is 1.3 α-helical turns further along the E-helix. The valine-to-histidine substitution positions the histidine N$^{\epsilon 2}$ atom at the correct Fe bonding distance so that no structural movements are required for hemichrome formation in oMb(H64V/V68H)·bishis·HS7.1. Consistent with this reasoning are the results from a very recent NMR structure for a hemichrome hemoglobin from the cyanobacterium *Synechocystis* sp. PCC 6803, in which the distal histidine is located at E10 (*37*). Superposition analysis of this monomeric hemoglobin versus nsHb·bishis·HS7.8 shows that the E- and F-helices are significantly closer together in nsHb·bishis·HS7.8 (*37*).

In contrast to the structural similarities discussed above, an aspect of the published hemichrome structures that shows considerable variation is the conformation of the CD corner. We find that hemichrome formation in equine hemoglobin is associated with the formation of a short helix in the CD corner of the α subunits. This CD helix is positioned between the C- and E-helices with only one or two intervening residues (the D-helix that occurs in myoglobin and hemoglobin *β* chains is missing in α chains). When Mitchell et al. (*25*) compared the *C. arenicola* hemichrome hemoglobin scHb·bishis·PEG8.0 with cyanomet "Hb-D" (a very similar hemoglobin from *C. arenicola*), they noted that a short helical segment in the CD corner region of scHb·bishis·PEG8.0 corresponded to an extended loop in cyanomet Hb-D. They concluded that this difference was most likely due to "the ligand state of the heme" and not to small sequence differences. Thus hemichrome coordination in scHb·bishis·PEG8.0 also may be associated with helix formation, but in this case the helix seems to be located in the position normally occupied by the D-helix, just before the E-helix with a loop of 8 intervening residues between it and the C-helix. In the case of rice hemoglobin nsHb·bishis·HS7.8, the region between the C- and E-helices consists solely of a long, highly mobile, loop (*26*). The CD corner of the hemichrome *β* subunits of antarctic fish hemoglobin tnHb·CO/bishis·PEG7.4 exists as a flexible loop, as it does in the *β* subunits of all vertebrate hemoglobins, but in this case it appears to be more disordered than normal since residues CD2 through CD12 were not visible at all in the electron density map and therefore not included in the final atomic model (*27*). Thus a variety of secondary structures between the C- and E-helices are compatible with hemichrome coordination. In all cases, however, the interactions between the residues in this region and the heme group are greatly reduced. This increases the mobility of the heme group, allowing it to shift to a more exposed position as the E- and F-helices move toward each other.

Functional Roles of Hemichrome Coordination. Although the recent literature has shown that monomeric hexacoordinate hemoglobins are fairly common (*38*), the functional roles of these proteins are unclear. It has been suggested that hexacoordination in monomeric hemoglobins may be a way of regulating the kinetics of ligand binding (*39*, *40*), scavenging NO (*26*, *41*), or sensing gases (*42*).

In the case of tetrameric mammalian hemoglobins, hemichromes usually have been associated with intermediates formed during the unfolding of wild-type hemoglobin under denaturing conditions or the unfolding of unstable mutant hemoglobins under less severe conditions (*43*, *44*). However, rapid-freezing techniques used in conjunction with EPR and Mössbauer spectroscopic methods have detected the presence of bishistidine complexes in solutions of native Fe(III) methemoglobin (i.e., hemichrome hemoglobin) as well as

in solutions of Fe(II) oxyhemoglobin (referred to as hemochrome hemoglobin) under physiological conditions (*44*, *45*). Supporting the experimental findings is a recent molecular dynamics simulation, carried out on methemoglobin, that replicated the formation of bishistidine complexes (*46*). This theoretical calculation predicted, remarkably, that distal histidine−Fe coordination would occur preferentially in the α-chain with a concomitant rearrangement of the α CD corner. Our crystallographic results are in very good agreement with the computational predictions.

Observation of hemichrome coordination in solution and in several crystal structures, along with the supporting theoretical simulation, shows that hemichrome complexes are energetically accessible substates of native hemoglobin, and this raises the question of possible functional roles for hemichrome complexes. Rifkind et al. (*44*) suggested that hemichromes could function in vivo in the degradation of hemoglobin and in the cooperative pathway of ligand binding to hemoglobin. Hemoglobin degradation is thought to occur in vivo via the formation of so-called Heinz bodies. Heinz body formation involves the copolymerization of hemichrome hemoglobin with the cytoplasmic domain of band 3, the most abundant erythrocyte membrane protein (*47*−*49*). The polymerization reaction is very specific for hemichrome hemoglobin as it does not occur with deoxyhemoglobin, oxyhemoglobin, or methemoglobin (*48*). Moreover, the mode of hemichrome hemoglobin−band 3 interaction is very different from the interaction of band 3 with liganded and deoxyhemoglobin. Normally the polyanionic NH_2-terminal peptide of a band 3 subunit interacts with the anion binding site in the central cavity of the hemoglobin tetramer to form a 1-to-1 complex (*50*−*52*). The hemichrome hemoglobin−band 3 complex, in contrast, consists of two hemoglobin tetramers per band 3 subunit (*49*), and although it involves the NH_2-terminal peptide of band 3 (*48*, *53*), it does not involve hemoglobin's anion binding site (*49*). The generation of a hemichrome complex in our crystals of horse hemoglobin includes an extensive rearrangement of the crystal lattice and the formation of a large tetramer−tetramer interface (Figure 1B). If a similar dimer of tetramers forms in vivo as a Heinz body component, this could account for the observed 2-to-1 stoichiometry of the hemichrome hemoglobin−band 3 complex.

In the case of hemichrome involvement in ligand binding, Rifkind et al. (*44*) suggested that some published results were indicative of the "possibility that the distal histidine may actually facilitate ligand binding". However, mutagenesis studies by Nagai et al. (*54*) showed that replacing the distal histidine of the *β* subunits of human hemoglobin with glutamine has only a modest influence on the structure and oxygen binding properties of hemoglobin. Similarly, Mathews et al. (*55*) found that substituting glutamine for His63(E7)*β* has no significant effect on carbon monoxide binding to R state hemoglobin tetramers, and substituting glutamine for His58(E7)α increases the association rate constant and the association equilibrium constant of carbon monoxide binding to R state hemoglobin tetramers by only a factor of 2. It would appear, therefore, that hemichrome formation has little if any role in ligand binding in human hemoglobin.

Another possible functional role for hemichrome complexes is in the in vivo reduction of methemoglobin. Under physiological conditions, and in the absence of a reducing system, oxyhemoglobin is converted to aquomethemoglobin at a rate of about 2% per day (*43*). In the red cell, the Fe^{3+} heme groups of nonfunctional methemoglobin are reduced to the functionally active Fe^{2+} state by an electron transfer reaction that requires reduced cytochrome b_5, a small bishistidine-coordinated cytochrome (*56*, *57*). Recent experimental and computational studies indicate that methemoglobin and cytochrome b_5 do not interact to form a unique stable complex. Rather, they form an ensemble of transient weak complexes of which only a small subset results in efficient electron transfer (*58*, *59*). Two characteristics of the most productive methemoglobin−cytochrome b_5 complexes are short heme−heme interaction distances and interactions involving the heme propionate groups (*58*, *59*). Thermodynamic data of the interaction of methemoglobin with cytochrome b_5 led Mauk and Mauk (*60*) to conclude that methemoglobin is likely to undergo a significant change in conformation on forming a complex with cytochrome b_5. Moreover, they suggested that this conformational change could include the formation of hemichrome subunits in methemoglobin because electron transfer between iron porphyrins that are both low spin (e.g., a bishistidine heme to bishistidine heme electron transfer) should be favored (*60*, *61*).

Key features of the eHb·bishis/met·HS5.4 structure support the hypothesis that hemichrome complexes play a role in the in vivo reduction of methemoglobin. In particular, the transition from aquomet α subunits to bishistidine α subunits is accompanied by an ∼1.2 Å movement of the α heme groups to a more solvent-exposed position. Normally, the α heme groups of liganded hemoglobin and deoxyhemoglobin have 115−120 $Å^2$ of their surface exposed to solvent. In eHb·bishis/met·HS5.4, α heme exposure is increased to 198 $Å^2$. By increasing the steric accessibility of the α heme groups, hemichrome formation should increase significantly the number of transient methemoglobin−cytochrome b_5 complexes with short heme−heme contacts. The general theory of Marcus (*62*) and the Brownian dynamics simulations of Kidd et al. (*59*) predict that decreasing the distance between the redox centers greatly increases electron transfer efficiency.

Close heme−heme interaction occurs, in fact, in the eHb·bishis/met·HS5.4 crystal structure where α hemes on two adjacent tetramers interact via hydrogen-bonded propionic acid groups, implying that at least one of propionic acid groups is protonated in this crystal lattice. These two tetramers, which associate through a network of hydrogen bonds (Figure 8), are related by a crystallographic 2-fold axis that passes through the propionic acid−propionic acid hydrogen bond (Figure 1B). The α heme iron atoms on adjacent tetramers are only 18.8 Å apart. This type of heme−heme interface has been reported in two similar electron transfer proteins. It was first observed by Chen et al. (*63*) in the structure of flavocytochrome *c* sulfide dehydrogenase. This protein contains a 21 kDa diheme cytochrome subunit that consists of two cytochrome *c*-like domains that are related by a pseudo-dyad axis. Chen et al. noted that the two heme groups interact via an interdomain hydrogen bond between propionic acid groups and that the heme iron atoms are separated by 19.0 Å. Kadziola and Larsen (*64*) reported that the same type of heme−heme contact occurs in the structure of cytochrome c_4 (a diheme protein with a tertiary structure similar to that of the diheme subunit in flavocytochrome *c* sulfide dehydrogenase). They stated that a

pseudo-2-fold axis "passes through a short hydrogen bond between the two heme propionic acid groups, connecting the redox center of each domain" and noted that the Fe−Fe distance is 19.1 Å. Significantly, this type of hydrogen-bonded heme−heme interaction is predicted to result in a very efficient electron transfer pathway for the reduction of methemoglobin by cytochrome b_5 (*59*).

NOTE ADDED IN PROOF

It has come to our attention that Peterson-Kennedy et al. (*66*) have reported evidence of hemichrome formation in the α-subunits of human hemoglobin. Their optical and EPR spectroscopic measurements revealed α-subunit hemichrome formation in the $[\alpha(Fe^{3+})\beta(Zn)]_2$ metal−hybrid tetramer [but not β-subunit hemichrome formation in the $[\alpha(Zn)\beta(Fe^{3+})]_2$ tetramer] upon cooling below 260 K. They also found that photoinitiated intratetramer electron transfer between the β-subunit Zn protoporphyrin and the α-subunit Fe^{3+} heme is increased somewhat by hemichrome formation.

ACKNOWLEDGMENT

We thank Dr. Jeffery S. Kavanaugh for helpful discussions and for assistance in the final stages of REFMAC5 refinement.

REFERENCES

1. Boyes-Watson, J., Davidson, E., and Perutz, M. F. (1947) *Proc. R. Soc. London, Ser. A 191*, 83−132.
2. Perutz, M. F. (1954) *Proc. R. Soc. London, Ser. A 225*, 264−286.
3. Silva, M. M., Rogers, P. H., and Arnone, A. (1992) *J. Biol. Chem. 267*, 17248−17256.
4. Mueser, T. C., Rogers, P. H., and Arnone, A. (2000) *Biochemistry 39*, 15353−15364.
5. Baldwin, J., and Chothia, C. (1979) *J. Mol. Biol. 129*, 175−220.
6. Kavanaugh, J. S., Moo-Penn, W. F., and Arnone, A. (1993) *Biochemistry 32*, 2509−2513.
7. Shaanan, B. (1983) *J. Mol. Biol. 171*, 31−59.
8. Perutz, M. F. (1968) *J. Crystal Growth 2*, 54−56.
9. Riggs, A. (1981) *Methods Enzymol. 76*, 5−29.
10. Howard, A. J., Nielsen, C., and Xuong, N. H. (1985) *Methods Enzymol. 114*, 452−472.
11. Ladner, R. C., Heidner, E. J., and Perutz, M. F. (1977) *J. Mol. Biol. 114*, 385−414.
12. Brünger, A. T. (1992) *X-PLOR, version 3.1*, Yale University Press, New Haven, CT.
13. Hendrickson, W. A. (1985) *Methods Enzymol. 115*, 252−270.
14. Murshudov, G., Vagin, A. A., and Dodson, E. J. (1997) *Acta Crystallogr. D53*, 240−255.
15. Collaborative Computational Project (1994) *Acta Crystallogr. D50*, 760−763.
16. Cambillau, C. (1989) *Silicon Graphics Geometry Partners Directory*, p 61, Silicon Graphics, Mountain View, CA.
17. Jones, T. A. (1985) *Methods Enzymol. 115*, 157−171.
18. Borgstahl, G. E. O. (1992) Ph.D. Thesis, The University of Iowa.
19. Brünger, A. T. (1993) *Acta Crystallogr. D49*, 24−36.
20. Kavanaugh, J. S., Weydert, J. A., Rogers, P. H., and Arnone, A. (1998) *Biochemistry 37*, 4358−4373.
21. Gerstein, M., and Chothia, C. (1991) *J. Mol. Biol. 220*, 133−149.
22. Cox, J. M. (1967) *J. Mol. Biol. 28*, 151−156.
23. Yang, F., and Phillips, G. N., Jr. (1996) *J. Mol. Biol. 256*, 762−774.
24. Berisio, R., Sica, F., Lamzin, V. S., Wilson, K. S., Zagari, A., and Mazzarella, L. (2002) *Acta Crystallogr. D58*, 441−450.
25. Mitchell, D. T., Kitto, G. B., and Hackert, M. L. (1995) *J. Mol. Biol. 251*, 421−431.
26. Hargrove, M. S., Brucker, E. A., Stec, B., Sarath, G., Arredondo-Peter, R., Klucas, R. V., Olson, J. S., and Phillips, G. N., Jr. (2000) *Structure 8*, 1005−1014.
27. Riccio, A., Vitagliano, L., di Primo, C., Zagari, A., and Mazzarella, L. (2002) *Proc. Natl. Acad. Sci. U.S.A. 99*, 9801−9806.
28. Dou, Y., Admiraal, S. J., Ikeda-Saito, M., Krzywda, S., Wilkinson, A. J., Li, T., Olson, J. S., Prince, R. C., Pickering, I. J., and George, G. N. (1995) *J. Biol. Chem. 270*, 15993−16001.
29. Qin, J., La Mar, G. N., Dou, Y., Admiraal, S. J., and Ikeda-Saito, M. (1994) *J. Biol. Chem. 269*, 1083−1090.
30. Vojtechovsky, J., Chu, K., Berendzen, J., Sweet, R. M., and Schlichting, I. (1999) *Biophys. J. 77*, 2153−2174.
31. Creighton, T. E. (1993) *Proteins: Structure and Molecular Properties*, W. H. Freeman, New York.
32. Rajashankar, K. R., and S., R. (1996) *Protein Sci. 5*, 932−946.
33. Fodje, M. N., and Al-Karadaghi, S. (2002) *Protein Eng. 15*, 353−358.
34. Perutz, M. F. (1970) *Nature 228*, 726−739.
35. Kavanaugh, J. S., Chafin, D. R., Arnone, A., Mozzarelli, A., Rivetti, C., Rossi, G. L., Kwiatkowski, L. D., and Noble, R. W. (1995) *J. Mol. Biol. 248*, 136−150.
36. Gallivan, J. P., and Dougherty, D. A. (1999) *Proc. Natl. Acad. Sci. U.S.A. 96*, 9459−9464.
37. Falzone, C. J., Vu, B. C., Scott, N. L., and Lecomte, J. T. J. (2002) *J. Mol. Biol. 324*, 1015−1029.
38. Trent, J. T., III, and Hargrove, M. S. (2002) *J. Biol. Chem. 277*, 19538−19545.
39. Trent, J. T., III, Hvitved, A. N., and Hargrove, M. S. (2001) *Biochemistry 40*, 6155−6163.
40. Trent, J. T., III, Watts, R. A., and Hargrove, M. S. (2001) *J. Biol. Chem. 276*, 30106−30110.
41. Sun, Y., Jin, K., Mao, X., Zhu, Y., and Greenberg, D. A. (2001) *Proc. Natl. Acad. Sci. U.S.A. 98*, 15306−15311.
42. Arredondo-Peter, R., Hargrove, M. S., Sarath, G., Moran, J. F., Lohrman, J., Olson, J. S., and Klucas, R. V. (1997) *Plant Physiol. 115*, 1259−1266.
43. Bunn, H. F., and Forget, B. G. (1986) *Hemoglobin: Molecular, Genetic and Clinical Aspects*, W. B. Saunders, Philadelphia, PA.
44. Rifkind, J. M., Abugo, O., Levy, A., and Heim, J. (1994) *Methods Enzymol. 231*, 449−480.
45. Levy, A., Kuppusamy, P., and Rifkind, J. M. (1990) *Biochemistry 29*, 9311−9316.
46. Ramadas, N., and Rifkind, J. M. (1999) *Biophys. J. 76*, 1796−1811.
47. Low, P. S., Waugh, S. M., Zinke, K., and Drenckhahn, D. (1985) *Science 227*, 531−533.
48. Waugh, S. M., and Low, P. S. (1985) *Biochemistry 24*, 34−39.
49. Waugh, S. M., Walder, J. A., and Low, P. S. (1987) *Biochemistry 26*, 1777−1783.
50. Cassoly, R. (1983) *J. Biol. Chem. 258*, 3859−3864.
51. Walder, J. A., Chatterjee, R., Steck, T. L., Low, P. S., Musso, G. F., Kaiser, E. T., Rogers, P. H., and Arnone, A. (1984) *J. Biol. Chem. 259*, 10238−10246.
52. Demehin, A. A., Abugo, O. O., Jayakumar, R., Lakowicz, J. R., and Rifkind, J. M. (2002) *Biochemistry 41*, 8630−8637.
53. Kannan, R., Labotka, R., and Low, P. S. (1988) *J. Biol. Chem. 263*, 13766−13773.
54. Nagai, K., Luisi, B., Shih, D., Miyazaki, G., Imai, K., Poyart, C., De Young, A., Kwiatkowsky, L., Noble, R. W., and Lin, S. H. (1987) *Nature 329*, 858−860.
55. Mathews, A. J., Rohlfs, R. J., Olson, J. S., Tame, J., Renaud, J. P., and Nagai, K. (1989) *J. Biol. Chem. 264*, 16573−16583.
56. Hultquist, D. E., and Passon, P. G. (1971) *Nature, New Biol. 229*, 252−254.
57. Durley, R. C. E., and Mathews, F. S. (1996) *Acta Crystallogr. D52*, 65−76.
58. Naito, N. R., Hui, H. L., Noble, R. W., and Hoffman, B. M. (2001) *Biochemistry 40*, 2060−2065.
59. Kidd, R. D., Baker, E. N., and Brittain, T. (2002) *J. Biol. Inorg. Chem. 7*, 23−30.
60. Mauk, M. R., and Mauk, A. G. (1982) *Biochemistry 21*, 4730−4734.
61. Pasternack, R. F., and Spiro, E. G. (1978) *J. Am. Chem. Soc. 100*, 968−972.
62. Marcus, R. A., and Sutin, N. (1985) *Biochim. Biophys. Acta 811*, 265−322.
63. Chen, Z.-w., Koh, M., Van Driessche, G., Van Beeumen, J. J., Bartsch, R. G., Meyer, T. E., Cusanovich, M. A., and Mathews, F. S. (1994) *Science 266*, 430−432.
64. Kadziola, A., and Larsen, S. (1997) *Structure 5*, 203−216.
65. Hyde, C. C., Rogers, P. H., Briley, P. D., and Arnone, A. (1984) in *Peptide and Protein Reviews* (Hearn, M. T. W., Ed.) pp 47−113, Marcel Dekker, New York.
66. Peterson-Kennedy, S. E., McGourty, J. L., Kalweit, J. A., and Hoffman, B. M. (1986) *J. Am. Chem. Soc. 108*, 1739−1746.

BI030059T